NANOSYSTEMS:
PHYSICS, CHEMISTRY, MATHEMATICS

Original article

Shutilov A.A., et al. *Nanosystems: Phys. Chem. Math.*, 2025, **16** (1), 30–43.
http://nanojournal.ifmo.ru
DOI 10.17586/2220-8054-2025-16-1-30-43

Design of highly active $Ni_xCo_{1-x}Al_2O_4$ ($x = 0.1 – 0.5$) catalysts for the dry reforming of methane reaction

Alexey A. Shutilov[1,a], Mikhail N. Simonov[1,2,b], Valeria E. Fedorova[1,c], Alexander S. Marchuk[2,d], Igor P. Prosvirin[1,e], Galina A. Zenkovets[1,f]

[1]Boreskov Institute of Catalysis SB RAS, Novosibirsk, Russia
[2]Novosibirsk State University, Novosibirsk, Russia

[a]alshut@catalysis.ru, [b]smike@catalysis.ru, [c]valeria@catalysis.ru, [d]alexander.s.marchuk@gmail.com, [e]prosvirin@catalysis.ru, [f]zenk@catalysis.ru

Corresponding author: Alexey A. Shutilov, alshut@catalysis.ru

ABSTRACT On the first step using co-precipitation method from Ni-, Co-, Al-containing solution a precipitates with a general composition of $Ni_xCo_{1-x}Al_2O_4$ ($x = 0.1 – 0.5$) were prepared. Calcination the obtained precipitates at 700 °C in air makes the precursors of catalysts for DRM with a stable spinel-like framework in which nickel and cobalt species are homogeneously incorporated. Reduction of the precursors at 700 °C in H_2 and further work under reaction medium leads to formation of the active phase which represents by the ensembles of Ni–Co alloy nanoparticles located on the surface of nanostructured spinel. The effect of the catalysts composition on catalytic properties in DRM was investigated. The high and stable catalytic activity of representative samples in DRM conditions with extremely short contact time ($\tau = 30$ ms) due to the formation of 17 – 18 wt. % active phase which represents highly dispersed (3 – 4 nm) Ni–Co alloy nanoparticles stabilized on the spinel with nanocristalline structure.

KEYWORDS sustainable environment, CH_4 and CO_2 utilization, dry reforming of methane (DRM), Ni–Co nanoalloy, spinel-based catalysts

ACKNOWLEDGEMENTS The authors express their gratitude to Ph. D. Olga A. Stonkus for studying catalysts using the TEM method and Ph. D. Vladimir A. Rogov for studying catalysts using the TPR-H_2 method. The study was funded by Russian Science Foundation according to the research project No. 23-23-10054, https://rscf.ru/project/23-23-10054/, and by the Government of Novosibirsk region contract 000000540699599823512080 2/ No. p-72.

FOR CITATION Shutilov A.A., Simonov M.N., Fedorova V.E., Marchuk A.S., Prosvirin I.P., Zenkovets G.A. Design of highly active $Ni_xCo_{1-x}Al_2O_4$ ($x = 0.1 – 0.5$) catalysts for the dry reforming of methane reaction. *Nanosystems: Phys. Chem. Math.*, 2025, **16** (1), 30–43.

1. Introduction

Today the dependence of humanity on fossil fuels has resulted in detrimental effects of growing emission of greenhouse gases, such as CO_2 and CH_4 [1], major contributors to climate change and resulting increase to the global temperature. Therefore, there is an urgency to control these emissions. Dry reforming of methane (DRM) is environmentally friendly catalytic transformation methane and carbon dioxide to syngas (1):

$$CH_4 + CO_2 = 2CO + 2H_2 \quad (\Delta_r H^o = 247.3\ \mathrm{kJ/mol}) \tag{1}$$

Due to a molar ratio of H_2/CO is close to 1, this is suitable for the synthesis of oxygenated chemicals and long chain hydrocarbons via Fisher–Tropsch synthesis [1–7]. Reaction (1) is also an attractive way to catalytically generate hydrogen-containing gas and can be used for hydrogen production [8]. In light of the energy applications, DRM formed H_2 + CO mixture is a very suitable fuel for intermediate and high temperatures solid oxide fuel cells for electricity production [9].

Among a large number of investigated catalysts for DRM, supported noble metals (Rh, Ru, Pd, Pt, Ir) can provide high and stable catalytic properties without sintering and coking of the catalysts during the reaction conditions [7, 10–13]. However, from an industrial standpoint, they are unsuitable for commercial use due to their high cost and limited availability. Therefore, it is more practical to develop non-noble metal-based catalysts [1, 2, 11]. It was shown that transitions metals Ni, Co, Fe, Cu and Mo supported on common supports such as γ-Al_2O_3, MgO, SiO_2, CeO_2 and ZrO_2 are alternatives to the catalysts for DRM, containing noble metals. Among that Ni containing catalysts are the most studded due to their high activity closed to noble metals [1, 2, 14, 15]. Thanks to the easy availability and low cost of γ-Al_2O_3, MgO, SiO_2, CeO_2 and ZrO_2, they have been widely studied for the DRM catalysts. Supports are not catalytically active

but interact with the active site to facilitate dispersion of metal, strengthen the metal-support interaction, limit sintering, accelerate reduction of the catalyst, and decrease or eliminate carbonaceous species development [12]. Due to low price, affordability and very good activity Ni-based catalysts may be used for the DRM reaction. However, these catalysts are prone to deactivation due to carbon deposition, as well as sintering of Ni nanoparticles under DRM conditions, that is the major drawback in the development of stable Ni-based catalysts [16–27].

To increase the activity and stability of supported Ni-based catalysts Co often has been used as an additive in these catalysts [11, 28–38]. Today, Ni–Co bimetallic catalysts have been widely explored as potential catalysts for use in DRM due to their advantages in activity and low cost [1, 33–37]. Thus, highly active and stable Ni–Co/Al_2O_3 catalyst for DRM reaction was reported by Wu et al.in [36]. The high catalytic performance they attribute to the formation of Ni–Co alloy under reaction conditions. Due to the similar Co and Ni electronic configuration, bimetallic Ni–Co alloyed nanoparticles are easily formed during the DRM reaction. Investigation of these catalysts by EXAFS and microscopic analysis revealed the lattice-strained configuration for the Ni–Co alloy and confirmed the strong interaction between Ni and Co atoms. The average bond lengths between the metal atoms in the bimetallic catalysts are some different compared to those in the parent metals, resulting in changes of the chemisorption properties [39]. Ni and Co easily form alloyed nanoparticles, and thus exhibiting a synergistic effect on one another. In literature extensive investigations of combinations between Ni and Co have been carried out for DRM. It has been reported that incorporation of Co into Ni catalysts inhibits the agglomeration of the nickel particles due to the formation of Ni–Co alloy and leads to an increased dispersion of the Ni particles [1, 11, 27].

In continuous efforts to develop Ni-based catalysts with the lowest carbon deposition and sustainable catalytic activity, the catalyst preparation process, including the metal loading percentage, calcination temperature, and reduction temperature on the catalytic properties are investigated today. It was shown [1, 2, 11, 12, 40, 41] that catalysts synthesis methods significantly affect catalysts activity in DRM. Impregnation, precipitation and co-precipitation, sol-gel, hydrothermal method, solvothermal method, microwave method, atomic layer deposition (ALT), sonochemical method, solution combustion are discussed. It was reported that catalysts prepared by a simple impregnation method have lower surface area compared to catalysts synthesized with sol-gel method due to pore blockage of the support by metal particles. Similar results were obtained in [11, 12] for catalysts prepared with sol-gel method in which Ni was highly dispersed on support with the strong metal-support interaction. The importance of the synthesis method was also reported by Wu et al. [36] who investigated the simultaneous and consecutive impregnation of the active phases (Ni and Co) on Al_2O_3 support for the DRM reaction. The authors concluded that the second method resulted in stronger Co-Ni interactions, which favored carbon gasification.

Our work proposed promising directions for the development of highly active and coke resistant catalysts for stable work in DRM. It was carried out a comprehensive investigation of the stage formation the structure of precursor of catalysts for DRM with a general composition of $Ni_xCo_{1-x}Al_2O_4$ ($x = 0.1 - 0.5$) prepared by using co-precipitation method after calcination at 700 °C in air. Also it was studied that the reduction of the precursors at 700 °C in H_2 and under reaction conditions which leads to formation of the active phase which represents by the ensembles of Ni–Co alloy nanoparticles of 3 – 4 nm in size located on the surface of nanostructured spinel. The effect of the catalysts composition on catalytic properties in DRM with extremely short contact time (τ) was investigated

2. Experimental

2.1. Catalyst preparation

Catalysts with a general composition of $Ni_xCo_{1-x}Al_2O_4$ ($x = 0.1 - 0.5$) were prepared by co-precipitation method. For comparison, $Co_1Al_2O_4$ sample was prepared too. Metal nitrate salts ($Ni(NO_3)_2 \cdot 6H_2O$, $Co(NO_3)_2 \cdot 6H_2O$ and $Al(NO_3)_3 \cdot 9H_2O$ (Vekton, Russia) were used as Ni, Co and Al precursors respectively. All reagents were used without additional purification. The required amounts of metal salts was dissolved in deionized water and then all individual solutions were mixed together to obtain the resulting solution, which was precipitated with 12.5 % solution of NH_4OH at pH = 7.5 and temperature of 75 °C. The precipitate was filtered, washed with deionized water and dried at room temperature and then dried overnight in air at 110 °C. The dried catalysts were calcined in static air at 700 °C for 4 h in a muffle furnace with a temperature ramp of 5 °C/min.

2.2. Catalyst characterization

Bulk chemical composition of the calcined catalyst was determined using a Perkin Elmer ISP OPTIMA 4300DV atomic emission spectrometer (Perkin Elmer, USA).

The specific surface area (S_{BET}) of the samples was determined by BET method using argon thermal desorption with a sorbtometr Sorby-M adsorption analyzer (META, Russia).

X-ray powder diffraction (XRD) analysis was carried out with Tongda TD3700 (Tongda, China) diffractometer using CuK_α-radiation and a Mythen2R 1D (Dectris, Switzerland) multistrip detector. Scanning was made over an angular range of 2θ = 5 – 70° at a 0.03° step and counting time of 3 s. Phase analysis, refinement of unite cell parameters and estimation of the quantitative content were performed by the full profile modeling of X-ray patterns by the Rietveld

method. The calculations were made using the TOPAS v.4.2 software package [42], structural parameters were taken from ICSD database [43]. Coherent scattering region (CSR) size was estimated by Rietveld method too.

In situ XRD analysis with H_2 atmosphere was made by using a Bruker D8 Advance diffractometer (Bruker, Germany), over an angular range of 2θ = 5 – 70° at a 0.03° step and counting time of 3 s. at each point using a LynxEye (1D) line detector. The monochromatic CuK_α-radiation ($\lambda = 1.5418$ Å) was used. The measurements were carried out using an XRK-900 high-temperature reactor chamber (Anton Paar, Austria). The 10 % H_2/ 90 % He mixture at a flow rate of 90 ml/min was passed through the chamber during heating or cooling to room temperature with a heating rate of 10 °C/min. The lattice parameters and phase relationships were refined with the Rietveld method.

The reducibility of the catalysts was studied by TPR-H_2 (temperature-programmed reduction) by 10 vol. % H_2 in Ar feed at flow rate of 40 ml/min during a linear temperature increase (10 °/min) in the range of 25 – 800 °C. Hydrogen consumption was determined by the heat conductivity detector of a Tsvet 500 chromatograph (Tsvet, Russia). Water was removed from the product by freezing at 77 K. The total H_2 consumption was calculated by integrating the area under the curve.

TEM (transmission electron microscopy) investigation was carried out using a JEM-2200FS transmission electron microscopy (JEOL Ltd., Japan, accelerating voltage 200 kV, lattice resolution $\sim$ 1 Å) equipped with a Cs-corrector. Dark-field images were obtained in a scanning mode using HAADF (High-Angle Annular Dark-Field) detector. The microscope is equipped with an EDX spectrometer (JEOL Ltd., Japan) for local elemental analysis (locality up to 1 nm, energy resolution -130 eV). Samples for the TEM study were prepared by ultrasonic dispersing in ethanol and subsequent deposition of the suspension upon a "holey" carbon film supported on a copper grid.

X-ray photoelectron spectra (XPS) were recorded on a SPECS spectrometer (SPECS, Germany) equipped with a PHOIBOS-150-MCD-9 analyzer and a FOCUS-500 monochromatic (MgK_α radiation, $h\nu = 1253.6$ eV, 150 W). The binding energy scale was calibrated using the levels of positions of the Au4$f_{7/2}$ ($E_b = 84.0$ eV) and Cu2$p_{3/2}$ peaks ($E_b = 932.67$ eV). Binding energy was calibrated against the position of the C1s peak ($E_b = 284.8$ eV), which corresponds to hydrocarbon deposits on the sample surface [44]. A sample in the form of a powder was deposited on a conductive double-sided copper adhesive tape. The survey spectrum and individual spectra of the elements were recorded at pass energy of the analyzer of 20 eV. The atomic ratios of the elements were calculated from the integral intensities of photoelectron peaks, which were corrected using appropriate sensitivity factors in terms of the Scofield photoionization cross sections [45]. The processing and analysis of the spectral data were conducted using the XPS Peak 4.1 software [46].

2.3. Catalytic tests

Catalytic tests were performed with 0.06 – 0.1 mm catalysts fraction in tubular quartz with an inner diameter of 4 mm which was installed in a furnace, where a thermocouple was placed into the annular space between the reactor and the furnace. Before the reaction, the catalysts were pretreated in a 10 vol % O_2/N_2 medium at 600 °C for 30 min with further reduction at 700 °C for 1 h in a 5 vol % H_2/He medium. In all cases, the DRM reaction was performed at a reaction mixture composition of (15 vol % CH_4 + 15 vol % CO_2) in N_2, the volumetric flow rate was 8 l/h, the volume of the loaded catalyst was 0.07 ml, a contact time (τ) was 30 ms, and temperatures of 500, 550, 600, 650 and 700 °C with exposure of the catalyst at each temperature for 30 min. The concentrations of the reagents and products were measured in the real-time regime on a Test-201 gas analyzer (Boner, Russia) equipped with IR optical, electrochemical, and polarographic sensors.

The catalyst performance was characterized by CH_4 conversion (X_{CH_4}, %), CO_2 conversion (X_{CO_2}, %), yield of H_2 (Y_{H_2}, %), and yield of CO (Y_{CO}, %), which were as follow:

$$X_{CH_4},\ \% = \frac{C^0_{CH_4} - C_{CH_4}}{C^0_{CH_4}} \cdot 100,$$

$$X_{CO_2},\ \% = \frac{C^0_{CO_2} - C_{CO_2}}{C^0_{CO_2}} \cdot 100,$$

$$Y_{H_2},\ \% = \frac{C_{H_2}}{2C^0_{CH_4}} \cdot 100,$$

$$Y_{CO},\ \% = \frac{C_{CO}}{C^0_{CO_2} + C^0_{CH_4}} \cdot 100,$$

where C^0_i , [vol. %] is the concentration of reagent at the inlet and C_i, [vol. %] – at the outlet of the reactor.

Due to the change in volume during the reaction, the conversion values calculated from volume concentrations are overestimated, which leads to a systematic error. In the conversion range from 10 % to 40 %, the relative error in determining the conversion is from 26.2 to 16.1 %. With increasing of conversion, the relative error decreases and at $X = 80$ % does not exceed 4.8 %.

Long-term tests for all investigated catalysts were carried out at 700 °C for 20 hours under DRM medium.

3. Results and discussion

3.1. Catalytic properties

The catalytic properties of obtained catalysts $Ni_xCo_{1-x}Al_2O_4$ ($x = 0.1 – 0.5$) and comparison sample $Co_1Al_2O_4$ were investigated in dry reforming of methane reaction under the identical reaction conditions. In Fig. 1 the influence of the reaction temperature on the methane (X_{CH_4}) and carbon dioxide (X_{CO_2}) conversion, on the hydrogen yield (Y_{H_2}) and on the molar ratio of H_2/CO are presented for all catalysts under investigation. It can be seen that activity of all catalyst as well as hydrogen production are increased with increasing reaction temperature from 500 to 700 °C, which is in accordance with the strong endothermic character of the dry reforming of methane reaction [2].

It can be seen that the monometallic $Co_1Al_2O_4$ catalyst is less active compare to bimetallic $Ni_xCo_{1-x}Al_2O_4$ catalysts. In the case of $Co_1Al_2O_4$ catalyst at 700 °C $X_{CH_4} = 61$ %, $X_{CO_2} = 62$ %, and the hydrogen yield $Y_{H_2} = 32$ %, H_2/CO = 0.62. A comparison of the bimetallic samples with each other shows that catalytic activity is increased with increasing the nickel content in the catalysts. At the reaction temperature of 700 °C increase the x value in catalyst $Ni_xCo_{1-x}Al_2O_4$ from 0.1 to 0.5 leads to increase in the X_{CH_4} from 64 to 77 %, the X_{CO_2} from 65 to 76 %, the Y_{H_2} from 32 to 42 % and H_2/CO ratio from 0.63 to 0.69.

The rather low the values of H_2/CO due to the reverse water gas shift reaction [2]:

$$CO_2 + H_2 = CO + H_2O. \tag{2}$$

According to the eq. (2), hydrogen reacts with CO_2 and CO and H_2O are formed. It leads to decrease in H_2/CO ratio in the reaction product compared to theoretical value H_2/CO = 1.

All investigated catalysts passed the long-term tests for study of stability in DRM medium without loss of catalytic activity (Table 1). Fig. 1(f) presents the results obtained during 20 hours of DRM reaction at 700 °C for the representative samples $Ni_{0.35}Co_{0.75}Al_2O_4$ and $Ni_{0.1}Co_{0.9}Al_2O_4$ catalysts.

TABLE 1. Catalytic properties of $Ni_xCo_{1-x}Al_2O_4$ samples ($x = 0.1 – 0.5$) and the comparison sample $Co_1Al_2O_4$ after 20 hours in the dry reforming of methane reaction at 700 °C

Sample	X_{CH_4}, %	X_{CO_2}, %	Y_{H_2}, %	Y_{CO}, %	H_2/CO, mole/mole	Result of long-term test
$Co_1Al_2O_4$	61	62	32	49	0.62	passed
$Ni_{0.1}Co_{0.9}Al_2O_4$	64	65	34	52	0.63	passed
$Ni_{0.25}Co_{0.75}Al_2O_4$	71	70	38	57	0.67	passed
$Ni_{0.35}Co_{0.65}Al_2O_4$	76	73	40	59	0.68	passed
$Ni_{0.5}Co_{0.5}Al_2O_4$	77	76	42	61	0.69	passed

3.2. Structural features

According to X-ray fluorescence analysis, the chemical composition of the prepared catalysts corresponds to the calculated one.

The structural properties of the obtained catalysts heated at 700 °C in air presented in Table 2 and Fig. 2. Based on the X-ray diffraction data, it may be seen that the phase composition of $Ni_xCo_{1-x}Al_2O_4$ (with $x = 0.1 – 0.5$) samples are the same. The main peaks located at $2\theta = 18.96$, 31.20, 36.76, 38.46, 48.97, 55.52, 59.22, 65.08° correspond to (111), (220), (311), (222), (331), (422), (511), (440) crystallographic planers of spinel structure Fm3m (ICSD-78407).

Unit cell parameter of spinel lattice is practically the same in all samples. It may be due to a very close values of ionic radius of Ni^{2+} and Co^{2+} (Ni^{2+} = 0.74 Å, Co^{2+} = 0.72 Å). But average size of a coherent scattering region (CSR) is some decreased from 12.69 to 9.54 nm with increasing the Ni concentration in spinel structure. The specific surface area of investigated samples is some increased from 109 to 128 m^2/g when the mole fraction of Ni varies within (0.1 – 0.5). It may be the reason of some reducing of particle size in the spinel structure when the mole fraction of Ni is increased, which is in a good agreement with XRD data.

Figure 3 shows electron microscopy images of a $Ni_{0.35}Co_{0.65}Al_2O_4$ catalyst calcined in air at a temperature of 700 °C. It can be seen that the sample consists of agglomerated particles of similar morphology with the size of 5 – 10 nm. EDX-element mapping analysis indicated the complete incorporation of Ni and Co in to the spinel lattice. That is in agreement with XRD investigations.

The structural characteristics of the catalysts after reaction presented in Table 3 and Fig. 4. In the $CoAl_2O_4$ catalyst spinel and pure metallic Co^0 phases were registered by XRD method. One can see the presence of spinel in comparison

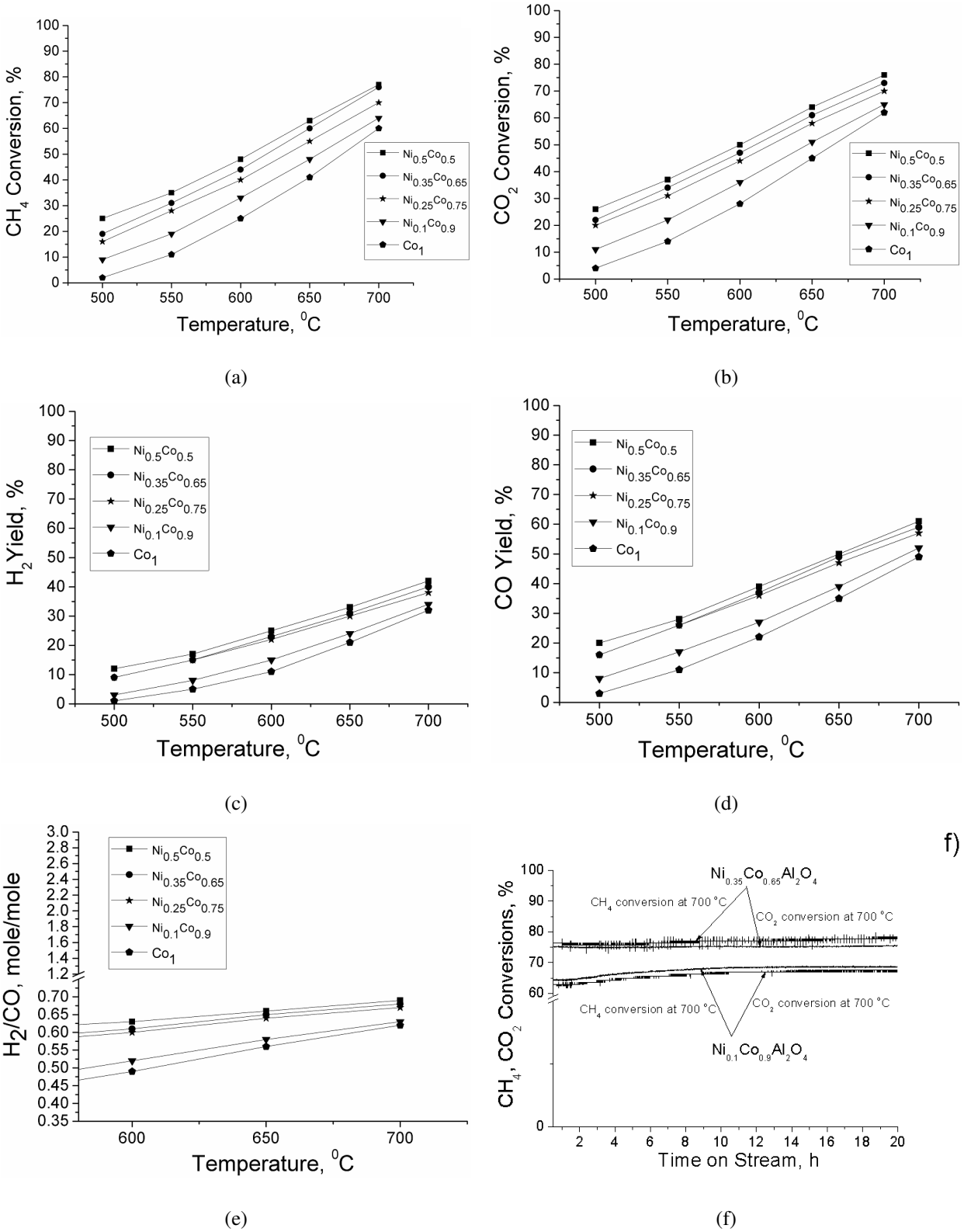

FIG. 1. CH_4 (a) and CO_2 (b) conversions, hydrogen yield (c), CO yield (d), molar ratio H_2/CO (e) and their corresponding equilibriums curves as a function of temperature in DRM over $Co_1Al_2O_4$, $Ni_{0.1}Co_{0.9}Al_2O_4$, $Ni_{0.25}Co_{0.75}Al_2O_4$, $Ni_{0.35}Co_{0.65}Al_2O_4$, $Ni_{0.5}Co_{0.5}Al_2O_4$ catalysts. And time on stream stability of DRM (f) over representative $Ni_{0.35}Co_{0.65}Al_2O_4$ and $Ni_{0.1}Co_{0.9}Al_2O_4$ catalysts

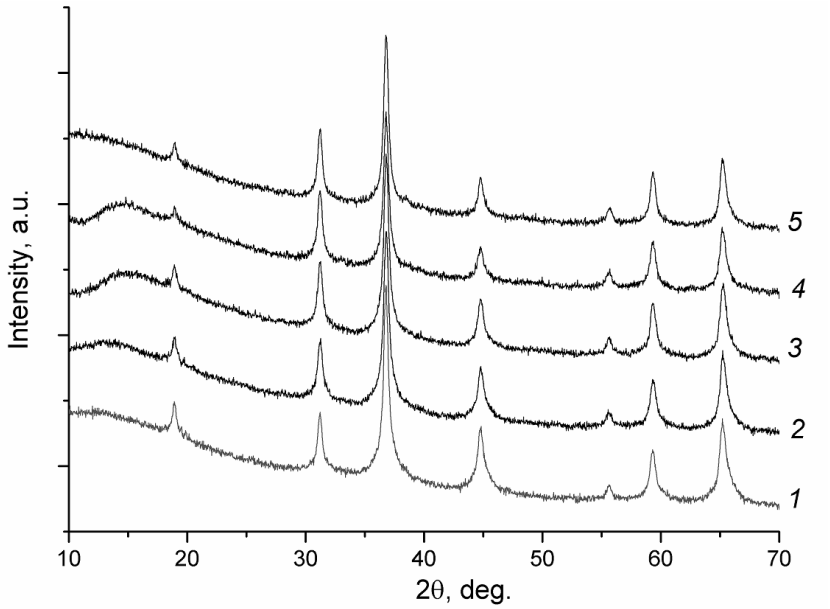

FIG. 2. X-ray patterns of $CoAl_2O_4$ (1), $Ni_{0.1}Co_{0.9}Al_2O_4$ (2), $Ni_{0.25}Co_{0.75}Al_2O_4$ (3), $Ni_{0.35}Co_{0.65}Al_2O_4$ (4), $Ni_{0.5}Co_{0.5}Al_2O_4$ (5) samples, heated in air at 700 °C

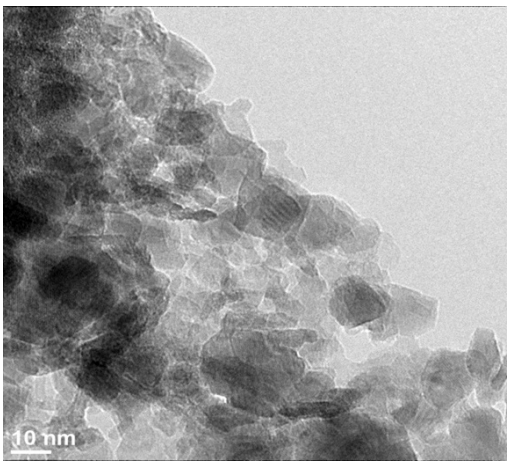

(a)

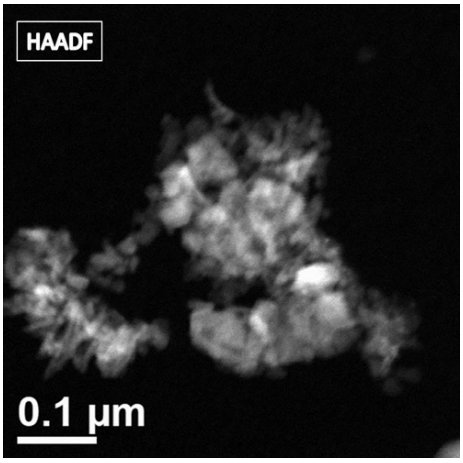

(b)

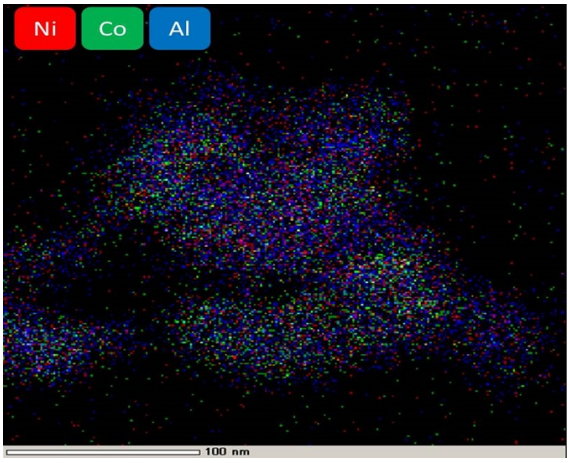

(c)

FIG. 3. TEM image (a), HAADF-STEM (b) image and corresponding EDX elemental mapping (c) of the representative $Ni_{0.35}Co_{0.65}Al_2O_4$ sample calcined in air at 700 °C

TABLE 2. Phase composition and structural properties of fresh catalysts $Ni_xCo_{1-x}Al_2O_4$ ($x = 0.1$ – 0.5) and the comparison sample $Co_1Al_2O_4$ heated at 700 °C in air

#	Sample	Phase	Lattice parameter, Å	CSR, nm	S_{BET}, m^2/g
1	$Co_1Al_2O_4$	Spinel	8.0939	12.69	116
2	$Ni_{0.1}Co_{0.9}Al_2O_4$	Spinel	8.0947	11.90	108.2
3	$Ni_{0.25}Co_{0.75}Al_2O_4$	Spinel	8.0914	11.48	108.8
4	$Ni_{0.35}Co_{0.65}Al_2O_4$	Spinel	8.0908	10.18	123.7
5	$Ni_{0.5}Co_{0.5}Al_2O_4$	Spinel	8.0943	9.54	127.6

TABLE 3. Phase composition and structural characteristics of $Ni_xCo_{1-x}Al_2O_4$ ($x = 0.1 – 0.5$) catalysts and the comparison sample $Co_1Al_2O_4$ after work in DRM media

#	Sample	Phase	Lattice parameter, Å	CSR, nm
1	$Co_1Al_2O_4$	Spinel (62 %)	8.042	3.62
		Co^0 (38 %)	3.540	3.99
2	$Ni_{0.1}Co_{0.9}Al_2O_4$	Spinel (83.5 %)	8.031	3.69
		(0.33Ni–0.77Co) alloy (16.5 %)	3.537	3.90
3	$Ni_{0.25}Co_{0.75}Al_2O_4$	Spinel (82.9 %)	8.049	3.06
		(0.3Ni–0.7Co) alloy (17.1 %)	3.539	3.67
4	$Ni_{0.35}Co_{0.65}Al_2O_4$	Spinel (82.3 %)	8.041	2.93
		(0.29Ni–0.71Co) alloy (17.7 %)	3.540	3.04
5	$Ni_{0.5}Co_{0.5}Al_2O_4$	Spinel (81.7 %)	8.039	3.89
		(0.42Ni–0.58Co) alloy (18.3 %)	3.530	3.75

sample $Co_1Al_2O_4$ and bimetallic Ni–Co alloy phase in $Ni_xCo_{1-x}Al_2O_4$ ($x = 0.1 – 0.5$) due to the shift of characteristics of the diffraction peaks at 2θ: 44.26 – 44.52°. The X-ray diffraction patterns of the Ni–Co alloy shows the diffraction peaks at 2θ: 44.26 – 44.52°, 51.57 – 51.58°, 75.92 – 76.44° which were attributed to the (111), (200), and (220) crystal planes of the Ni–Co alloy (ICSD-76632, ICSD-646088).

X-ray patterns of $Ni_{0.35}Co_{0.65}Al_2O_4$ catalyst at first heated in air at 700 °C and then in situ reduced in 10 % H_2/ 90 % He mixture in the temperature range of 200 – 700 °C presented in Fig. 5. It may be seen that the phase of intermetallic Ni–Co alloy is formed under the reduction at 620 °C and higher.

It is visible from the data presented in Table 3 that in $Co_1Al_2O_4$ sample the concentration of Co^0 metal phase is 38 %. In $Ni_xCo_{1-x}Al_2O_4$ samples the concentration of Ni–Co alloy metal phase is increased from 16.5 % to 18.3 % as x value increased from 0.1 to 0.5. At the same time Ni/Co ratio in bimetallic alloy does not change significantly (0.33/0.77; 0.3/0.7; 0.29/0.71) with x value increasing from 0.1 to 0.35. In a sample with $x = 0.5$ this value is increased to ratio $0.42/0.58$.

Despite the high reaction temperature, the rather high dispersion of catalysts particles are observed in investigated catalysts (Table 3). By comparison of data in Tables 2 and 3, one can see that the CSR value of spinel structure decreases from 10 – 11 to 3.0 – 3.5 nm. Simultaneously, the highly dispersed particles of Ni–Co nanoalloy with the average size of 3 – 4 nm are formed.

As can be seen from the HAADF-STEM image of $Ni_{0.35}Co_{0.65}Al_2O_4$ catalyst after work in the reaction mixture (Fig. 6a), the agglomerates of metal particles about 10 – 20 nm in size are observed on the surface of the spinel structure. This fact is inconsistent with the XRD data in (Table 3). According to element mapping data (Fig. 6b) the Ni–Co bimetallic alloy are formed. The formation of individual cobalt and nickel particles smaller than 1 nm on the surface cannot be ruled out. Fig. 6c show that under reaction condition cobalt and nickel leave the spinel structure, stabilized as nanodispersed Ni–Co alloy particles about 5 nm in size, collected in bigger aggregates on the outer surface, whereby the spinel structure becomes nanocrystalline. It consists of incoherently fused small spinel particles of 3 – 4 nm in size. In this case, the spinel CSR size decreases, but it lattice parameter does not change. This explanation agrees to the XRD results presented above. Due to the extraction of nickel and cobalt cations from the spinel structure under reducing conditions, their content in areas not containing metal particles decreases by about 1.5 times comparing to the initial catalyst.

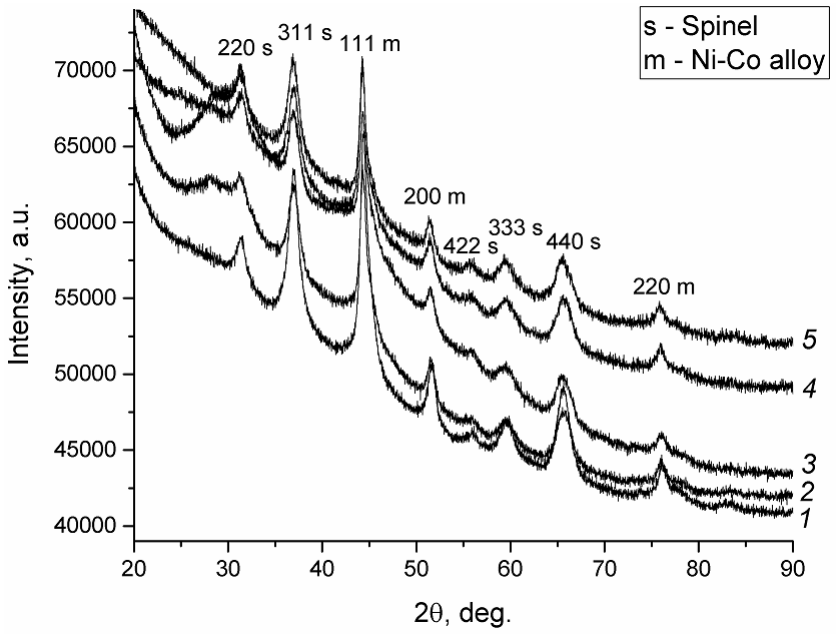

FIG. 4. X-ray patterns of $CoAl_2O_4$ (1), $Ni_{0.1}Co_{0.9}Al_2O_4$ (2), $Ni_{0.25}Co_{0.75}Al_2O_4$ (3), $Ni_{0.35}Co_{0.65}Al_2O_4$ (4), $Ni_{0.5}Co_{0.5}Al_2O_4$ (5) used catalysts with previous activation in hydrogen at 700 °C

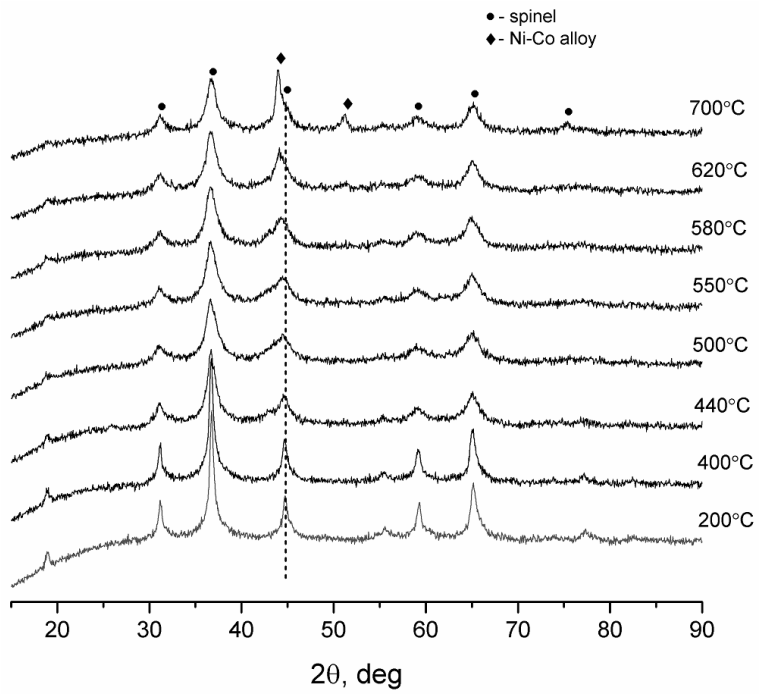

FIG. 5. X-ray patterns recorded during *in situ* reduction of representative $Ni_{0.35}Co_{0.65}Al_2O_4$ catalyst, previously heated at 700 °C in air

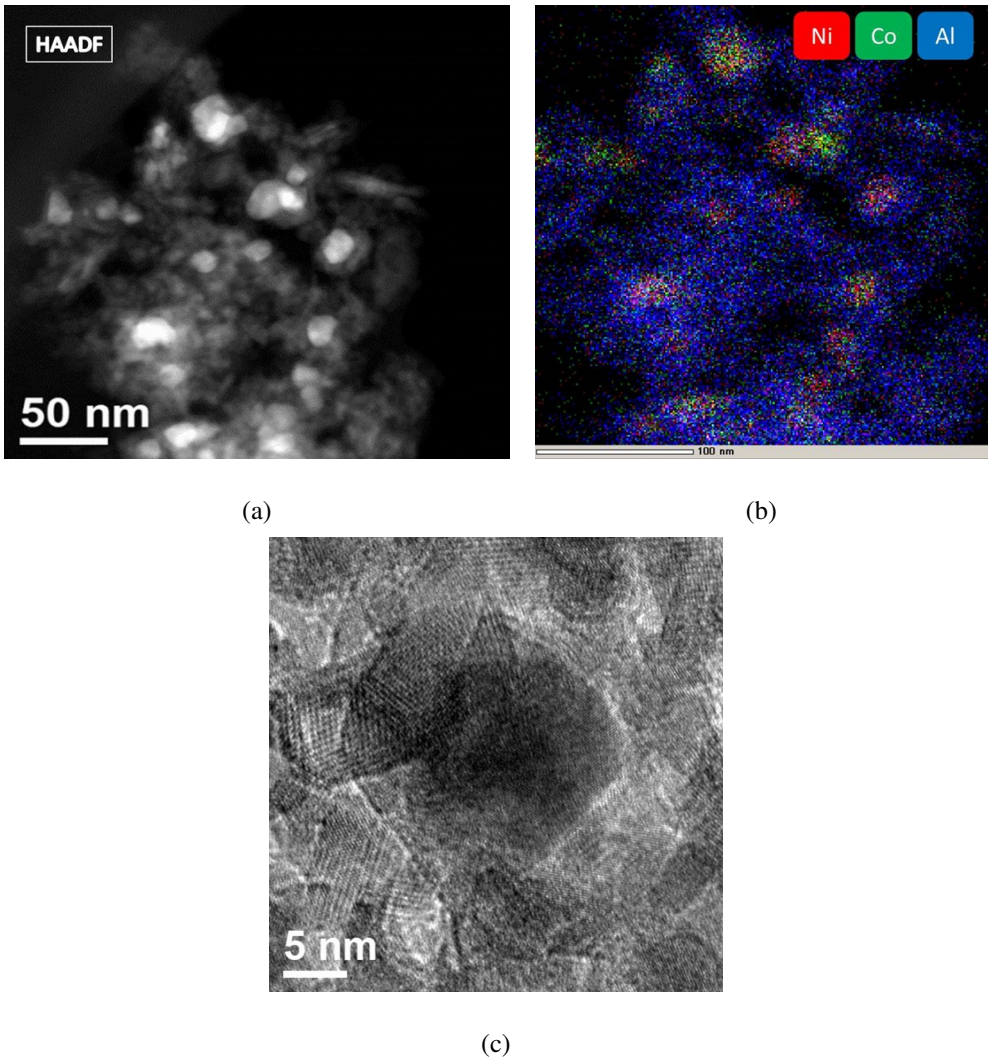

FIG. 6. HAADF-STEM image (a), EDX elemental mapping (b) and HRTEM (c) of the representative $Ni_{0.35}Co_{0.65}Al_2O_4$ sample after reaction

It was shown in the literature that formation of Ni–Co alloy configuration may exert a significant influence on the electronic properties of Ni–Co and thus benefit the catalytic properties [2, 36]. Certainly Ni–Co alloy is the active phase in DRM reaction. In our case, it is visible that increasing the concentration of Ni–Co alloy in $Ni_xCo_{1-x}Al_2O_4$ catalysts lead to increasing their catalytic activity in DRM.

3.3. Catalysts reducibility (TPR–H_2)

Before the reaction $Ni_xCo_{1-x}Al_2O_4$ ($x = 0.1 - 0.5$) catalysts and the comparison sample $Co_1Al_2O_4$ previously calcined at 700 °C in air, were activated by reduction of 5 vol. % H_2/He mixture at 700 °C for 1 h. In order to study the features of this activation, method of temperature-programed hydrogen reduction (TPR–H_2) was applied. Obtained TPR–H_2 profilers for all catalysts are shown in Fig. 7. For $CoAl_2O_4$ sample hydrogen consumption peaks can be distinguished at the temperature of 527, 670 and 774 °C. According to the literature [31, 47, 48] and XRD data in situ, the first peak at 527 °C can be identified as the reduction of surface Co^{3+} to Co^{2+}. The peak at 670 °C may be identified with the reduction of the part of Co^{3+} ions to Co^0 with formation of metal compound. The high temperature reduction peak at 774 °C may be associated with the reduction of some part of $Co^{(2,3)+}$ ions localized in strong interaction in the volume of the spinel structure.

For $Ni_xCo_{1-x}Al_2O_4$ ($x = 0.1 - 0.5$) series, in all samples also three regions of hydrogen consumption can be observed: 512 – 409 °C (I region), 631 – 587 °C (II region), and 784 – 812 °C (III region), whose positions are dependent on the Ni content. With increasing x value from 0.1 to 0.5 peaks observed in I and II regions slightly shift towards lower temperature ranges and peaks observed in region III some shift to higher temperature range. The value of H_2 consumption increases from 4.9 to 5.6 mlmol H_2/g with an increase in the nickel content in the samples from $x = 0$ to $x = 0.5$.

Based on the analysis of literature data [2, 28, 31, 47, 48] and the results of studying samples by XRD method, the H_2 consumption in the I temperature region may indicate the reducibility of Ni^{2+} to Ni^0 in (Ni–O–Co, Ni–O–Al) structures

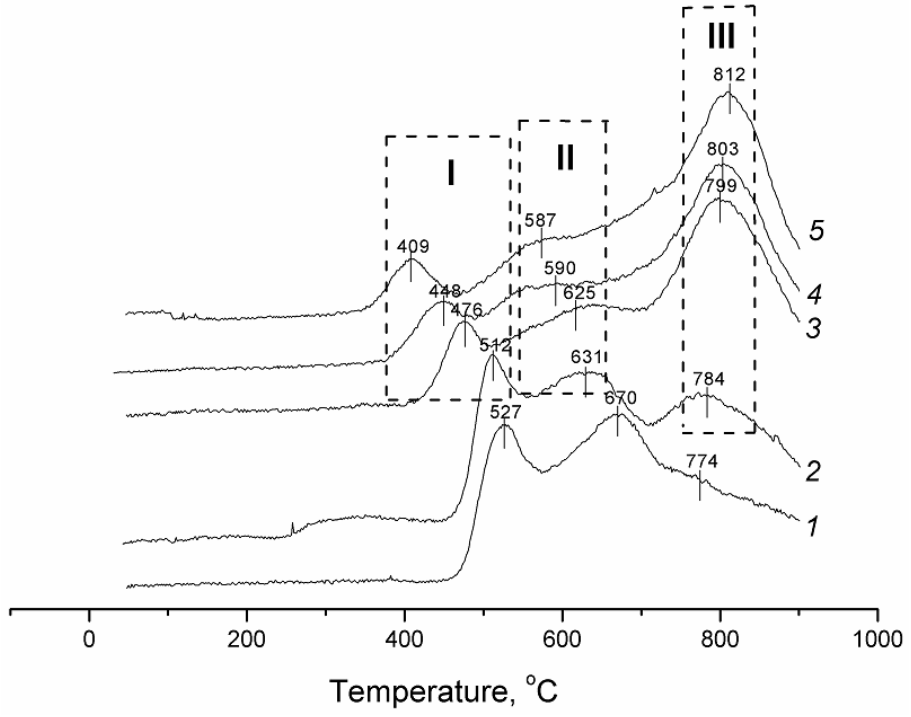

FIG. 7. TPR-H_2 profiles of $CoAl_2O_4$ (1), $Ni_{0.1}Co_{0.9}Al_2O_4$ (2), $Ni_{0.25}Co_{0.75}Al_2O_4$ (3), $Ni_{0.35}Co_{0.75}Al_2O_4$ (4), $Ni_{0.5}Co_{0.5}Al_2O_4$ (5) samples

localized on the surface of the spinel structure. Decreasing in Co^{3+} reduction temperature from 527 to 512 °C under addition of Ni to $CoAl_2O_4$ indicates the decreasing strength of the metal-support interaction in these catalysts [36]. This region of hydrogen uptake is associated with the reduction of Co^{3+} cations localized on the surface of spinel structure. The peaks in the region II may be due to the formation of Ni–Co alloy. This process becomes easier as the x value increases. According to [1, 2, 36], this shift indicates ease of reduction of the metallic oxides to the metallic forms. The high temperature reduction peak localized in III region may be associated with the reduction of some part of Co and Ni ions localized in strong interaction in the volume of the spinel structure [47].

Hence, the introduction of Ni into $CoAl_2O_4$ greatly changes their reducing properties. Thus, in the $Ni_xCo_{1-x}Al_2O_4$ samples, as a result of activation, reduction of Ni^{2+} and Co^{3+} cations on the surface of spinel structure lead to their exsolution and bimetallic alloyed Ni–Co nanoparticles are formed.

3.4. XPS study

Figure 8 presents the survey X-ray photoelectron spectrum of $Ni_{0.35}Co_{0.65}Al_2O_4$ sample heated in air at 700 °C. The surface composition of this sample corresponds to the declared one because no additional elements and contamination were detected. To investigate the valance states of individual elements the narrow spectral regions were analyzed. These spectra are presented in Fig. 9(a – d). One can see that binding energy (BE) of $Ni2p_{3/2}$ peak is 854.8 eV which corresponds to Ni^{2+} state [49, 50]. In Co2p spectrum peak position is 781.2 eV corresponding to Co^{2+} state [51, 52].

After reaction in the spectra of investigated sample in the spectral region of Ni2p additional shoulder with BE = 852.6 eV is appeared, which corresponds to Ni^0 state [44]. Simultaneous, in Co2p spectrum additional shoulder with BE = 778.2 eV is appeared. Such value of BE indicates the presence of Co^0 state [53]. The chemical state of alumina was carried out from Al2p peak position. In both samples (fresh and after reaction), the value of the BE of this peak is 74.3 eV and is characteristic of Al^{3+} state [54, 55]. XP spectra recorded in O1s region (Fig. 9d) indicate the peak at ∼531 eV due to O^- in the Al_2O_3 lattice.

Obtained results indicate that in fresh catalyst nickel is predominantly in the Ni^{2+} state and cobalt in Co^{2+} state, alumina in Al^{3+} state. In the catalyst after reaction nickel in Ni^0 state, cobalt in Co^0 state are appeared. In both samples Al^{3+} state is observed.

4. Conclusions

Highly active bimetallic Ni–Co catalysts supported on spinel-based structure with a general composition of $Ni_xCo_{1-x}Al_2O_4$ ($x = 0.1 - 0.5$) for DRM reaction were prepared by co-precipitation method. Preparation of the catalysts by precipitation method allow on the first stage to obtained precursors containing homogeneously distributed Ni and Co species in its volume, which on the further calcination at 700 °C in air spinel structure with homogeneous distribution of

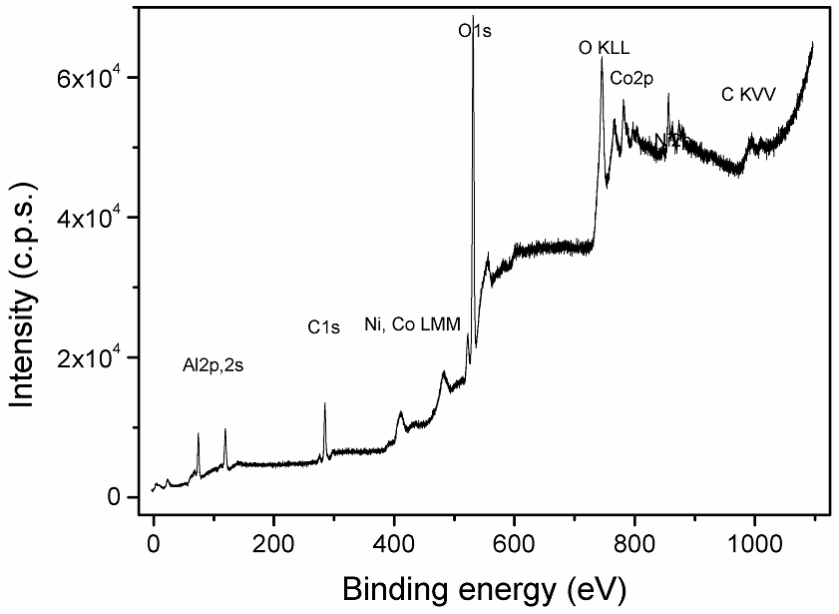

FIG. 8. Survey XP spectrum of the $Ni_{0.35}Co_{0.65}Al_2O_4$ catalyst before the reaction

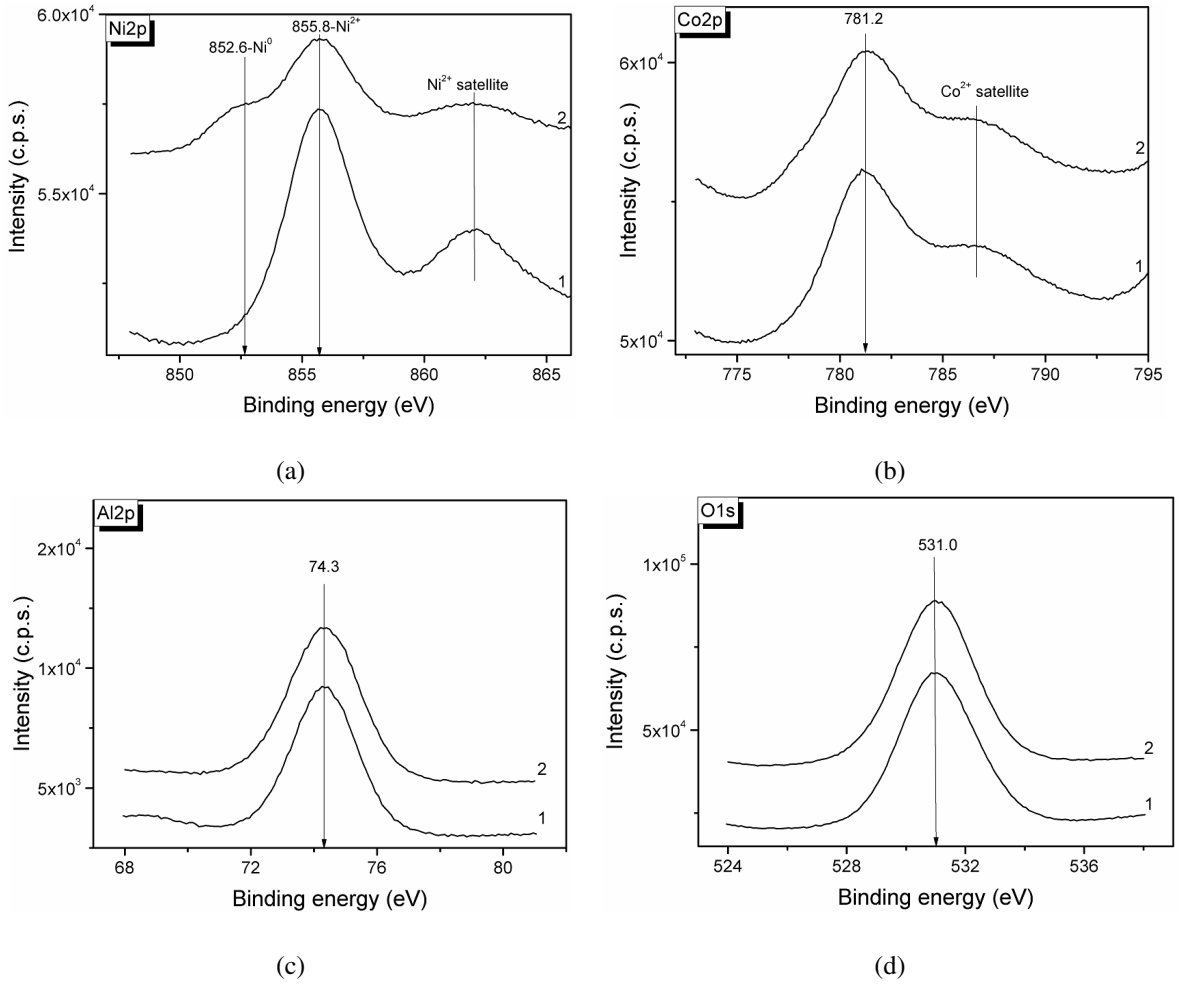

FIG. 9. Ni2p (a), Co2p (b), Al2p (c), O1s (d) spectra of representative $Ni_{0.35}Co_{0.65}Al_2O_4$ catalyst before (1) and after (2) reaction

Ni^{2+} and Co^{2+} ions in the spinel structure. During the reduction in H_2 or *in situ* reaction condition Ni^0 and Co^0 formed by the reduction can no longer stay in the spinel lattice, resulting in the migration to the surface to form the highly dispersed Ni–Co bimetallic alloy particles. It should be noted that under these catalytic conditions, not all nickel and cobalt are completely reduced to the metallic state in the spinel structure. The content of metal Ni–Co alloy particles is about 17 – 18 wt. %. The rest part of the nickel and cobalt remains stabilized in the spinel structure. According to the obtained and some literature data, it may be concluded that the high activity of this catalysts are due to the highly dispersed and stable Ni–Co alloy particles (3 – 4 nm in size) on the surface of spinel structure, from which the nickel and cobalt species partly evolve from the cations homogeneously distributed in spinel matrix. The synergy of Ni and Co in alloy bimetallic catalysts provides high activity with extremely short contact time ($\tau = 30$ ms) and high stability during time on steam in DRM reaction.

A comparison of experimental data obtained in this work for catalytic activity in the DRM reaction with literature analogues (Table 4) indicates the significant potential of the our catalysts among catalysts described in the literature.

TABLE 4. A comparison of experimental data obtained in this work for catalytic activity in the DRM reaction with literature analogues

#	Catalyst	Preparation method	DRM reaction conditions	Best performance achievements	Time of stream (TOS) stability	Ref.
1	3.37 % Co – 11.2 % $Ni/MgAl_2O_4$	Incipient wetness impregnation	18825 ml/g·h; CH_4:CO_2:N_2 = 1:1:3; 600 °C	X_{CH_4}= 9 %; X_{CO_2}=13 %; H_2/CO = 0.5	Only an initial slight drop of X_{CH_4}; X_{CO_2} after TOS 1.5 h	28
2	7.5 % Co – 7.5 % $Ni/MgAl_2O_4$	Incipient wetness impregnation	10000 ml/g·h; CH_4:CO_2:N_2 = 1:1:3; 600 °C	X_{CH_4}=16 %; H_2/CO = 0.45	A small decrease of X_{CH_4} in the first 90 min	38
3	8 % Co – 1 % Ni/Al_2O_3	Excess volume impregnation	22000 h^{-1} (GHSV); CH_4:CO_2 = 1:1 700 °C	X_{CH_4}=71 %; X_{CO_2}= 80 %	Deactivation after 6 h	37
4	$Ni_{0.375}Co_{0.375}Mg_{0.25}Al_2O_4$	Wet impregnation	60000 h^{-1} (GHSV) CH_4:CO_2:N_2 = 2.3:4.6:1 (20 ppm H_2S) 850 °C	X_{CH_4}=40 %; X_{CO_2}= 32 %	Performance decreases in the first 6 h	56
5	NiCoAlO	One pot evaporation-induced self-assembly	CH_4:CO_2 = 1; 700 °C	X_{CH_4}=52 %; X_{CO_2}= 60 %; H_2/CO = 0.82	—	57
6	Ni/Al_2O_3	Impregnation	12000 ml/g·h; 700 °C	X_{CH_4}=57 %; X_{CO_2}= 70 %	Performance decreases in the first 3 h	58
7	$Ni_{0.5}Co_{0.5}Al_2O_4$ (a); $Ni_{0.35}Co_{0.65}Al_2O_4$ (b)	Co-precipitation	120000 h^{-1} (GHSV) (15 % CH_4 + 15 % CO_2)/N_2 700 °C	X_{CH_4} =77 %; X_{CO_2} =76 %; H_2/CO = 0.69 (a); X_{CH_4} = 76 %; X_{CO_2} = 73 %; H_2/CO = 0.68 (b)	Stable performance for 20 h	This work

References

[1] Alipour Z., Borugadda V.B., Wang H., Dalai A.K. Syngas production through dry reforming: A review on catalysts and their materials, preparation methods and reactor type. *Chemical Engineering J.*, 2023, **452**, 139416.

[2] Yentekakis I.V., Panagiotopoulou P., Artemakis G. A review of recent efforts to promote dry reforming of methane (DRM) to syngas production via bimetallic catalyst formulations. *Appl. Catal. B: Environ.*, 2021, **296**, 120210.

[3] Zhang G., Liu J., Xu Y., Sun Y. A review of CH_4 CO_2 reforming to synthesis gas over Ni-based catalysts in recent years (2010–2017). *Int. J. Hydrogen Energy*, 2018, **43**, P. 15030–15054.

[4] Yentekakis I.V., Goula G., Hatzisymeon M., Betsi-Argyropoulou I., Botzolaki G., Kousi K., Kondarides D.I., Taylor M.J., Parlett C.M.A., Osatiashtiani A., Kyriakou G., Holgado J.P., Lambert R.M. Effect of support oxygen storage capacity on the catalytic performance of Rh nanoparticles for CO_2 reforming of methane. *Appl. Catal. B: Environ.*, 2019, **243**, P. 490–501.

[5] Abdulrasheed A., Jalil A.A., Gambo Y., Ibrahim M., Hambali H.U., Shahul Hamid M.Y. A review on catalyst development for dry reforming of methane to syngas: recent advances. *Renewable Sustainable Energy Rev.*, 2019, **108**, P. 175–193.

[6] Song Y., Ozdemir E., Ramesh S., Adishev A., Subramanian S., Harale A., Albuali M., Fadhel B.A., Jamal A., Moon D., Choi S.H., Yavuz C.T. Dry reforming of methane by stable Ni–Mo nanocatalysts on single-crystalline MgO. *Science*, 2020, **367**, P. 777–781.

[7] Pakhare D., Spivey J. A review of dry (CO_2) reforming of methane over noble metal catalysts. *Chem. Soc. Rev.*, 2014, **43**, P. 7813–7837.

[8] Su B., Wang Y., Xu Z., Han W., Jin H., Wang H. Novel ways for hydrogen production based on methane steam and dry reforming integrated with carbon capture. *Energy Convers. Manag.*, 2022, **270**, 116199.

[9] Yentekakis I.V., Goula G. Biogas management: advanced Utilization for Production of renewable energy and added-value chemicals. *Front. Environ. Sci.*, 2017, **5**, P. 7–18.

[10] Tsoukalou A., Imtiaze Q., Kim S.M., Abdala P.-M., Yoon S., Muller C.-R. Dry-reforming of methane over bimetallic Ni–M/La_2O_3 (M = Co, Fe): The effect of the rate of $La_2O_2CO_3$ formation and phase stability on the catalytic activity and stability. *J. Catal.*, 2016, **343**, P. 208–214.

[11] Bitters J.S., He T., Nestler E., Senanayake S.D., Chen J.G., Zhang C. Utilizing bimetallic catalysts to mitigate coke formation in dry reforming of methane. *J. of Energy Chemistry*, 2022, **68**, P. 124–142.

[12] Sharifianjazi F., Esmaeilkhanian A., Bazli L., Eskandarinezhad S., Khaksar S., Shafiee P., Yusuf M., Abdullah B., Salahshour P., Sadeghi F. A review on recent advances in dry reforming of methane over Ni- and Co-based nanocatalysts. *Int. J. Hydrog. Energy*, 2022, **47**, P. 42213–42233

[13] Rezaei M., Alavi S.M., Sahebdelfar S., Yan Z.F. Syngas production by methane reforming with carbon dioxide on noble metal catalysts. *J. Nat. Gas. Chem.*, 2006, **15**, P. 327–334.

[14] Barama S., Dupeyrat-Batiot C., Capron M., Bordes-Richard E., Bakhti-Mohammedi O., Catalytic properties of Rh, Ni, Pd and Ce supported on Al-pillared montmorillonites in dry reforming of methane. *Catal. Today*, 2009, **141**, P. 385–392.

[15] Ferreira-Aparicio P., Guerrero-Ruiz A., Rodriquez-Ramos I. Comparative study at low and medium reaction temperatures of syngas production by methane reforming with carbon dioxide over silica and alumina supported catalysts. *Appl. Catal. A: Gen.*, 1998, **170**, P. 177–187.

[16] Goula M.A., Charisiou N.D., Siakavelas G., Tzounis L., Tsiaoussis I., Panagiotopoulou P., Goula G., Yentekakis I.V. Syngas production via the biogas dry reforming reaction over Ni supported on zirconia modified with CeO_2 or La_2O_3 catalysts. *Int. J. Hydrog. Energy*, **42**, P. 13724–13740.

[17] Le Sach´e E., Pastor-P´erez L., Watson D., Sepúlveda-Escribano A., Reina T.R. Ni stabilised on inorganic complex structures: superior catalysts for chemical CO_2 recycling via dry reforming of methane. *Appl. Catal. B: Environ.*, 2018, **236**, P. 458–465.

[18] Serrano-Lotina A., Daza L. Long-term stability test of Ni-based catalyst in carbon dioxide reforming of methane. *Appl. Catal. A Gen.*, 2014, **474**, P. 107–113.

[19] Li X., Li D., Tian H., Zeng L., Zhao Z.-J., Gong J. Dry reforming of methane over Ni/La_2O_3 nanorod catalysts with stabilized Ni nanoparticles. *Appl. Catal. B: Environ.*, 2017, **202**, P. 683–694.

[20] Stroud T., Smith T.J., Le Sach´e E., Santos J.L., Centeno M.A., Arellano-Garcia H., Odriozola J.A., Reina T.R. Chemical CO_2 recycling via dry and bi reforming of methane using Ni-Sn/Al_2O_3 and Ni-Sn/CeO_2-Al_2O_3 catalysts. *Appl. Catal. B: Environ.*, 2018, **224**, P. 125–135.

[21] Makri M.M., Vasiliades M.A., Petallidou K.C., Efstathiou A.M., Effect of support composition on the origin and reactivity of carbon formed during dry reforming of methane over 5 wt % Ni/$Ce_{1-x}MxO_{2-\delta}$ (M = Zr^{4+}, Pr^{3+}) catalysts. *Catal. Today*, 2015, **259**, P. 150–164.

[22] Zhang W.D., Liu B.S., Tian Y.L. CO_2 reforming of methane over Ni/Sm_2O_3-CaO catalyst prepared by a sol–gel technique. *Catal. Comm.*, 2007, **8**, P. 661–667.

[23] Amin M.H., Mantri K., Newnham J., Tardio J., Bhargava S.K. Highly stable ytterbium promoted Ni/γ-Al_2O_3 catalysts for carbon dioxide reforming of methane. *Appl. Catal. B: Environ.*, 2012, **119**, P. 217–226.

[24] Zhang F., Liu Z., Zhang S., Akter N., Palomino R.M., Vovchok D., Orozco I., Salazar D., Rodriguez J.A., Llorca J., Lee J., Kim D., Xu W., Frenkel A.I., Li Y., Kim T., Senanayake S.D. In situ elucidation of the active state of Co–CeO_x catalysts in the dry reforming of methane: the important role of the reducible oxide support and interactions with cobalt. *ACS Catal.*, 2018, **8**, P. 3550–3560.

[25] Fakeeha A.H., Al Fatesh A.S., Ibrahim A.A., Kurdi A.N., Abasaeed A.E. Yttria modified ZrO_2 supported Ni catalysts for CO_2 reforming of methane: the role of Ce promoter. *ACS Omega*, 2021, **6**, P. 1280–1288.

[26] Kim S.M., Abdala P.M., Margossian T., Hosseini D., Foppa L., Armutlulu A., van Beek W., Comas-Vives A., Cop´eret C., Müller C. Cooperativity and dynamics increase the performance of NiFe dry reforming catalysts. *J. Am. Chem. Soc.*, 2017, **139**, P. 1937–1949.

[27] Kurlov A., Deeva E.B., Abdala P.M., Lebedev D., Tsoukalou A., Comas-Vives A., Fedorov A., Muller C.R. Exploiting two-dimensional morphology of molybdenum oxycarbide to enable efficient catalytic dry reforming of methane. *Nat. Comm.*, 2020, **11**, 4920.

[28] Sengupta S., Ray K., Deo G. Effects of modifying Ni/Al_2O_3 catalyst with cobalt on the reforming of CH_4 with CO_2 and cracking of CH_4 reactions. *Int. J. Hydrog. Energy*, 2014, **39**, P. 11462–11472.

[29] Gonzalez-delaCruz V.M., Pereniguez R., Ternero F., Holgado J.P., Caballero A. In situ XAS study of synergic effects on Ni–Co/ZrO_2 methane reforming catalysts. *J. Phys. Chem. C.*, 2012, **116**, P. 2919–2926.

[30] Son I.H., Lee S.J., Roh H-S. Hydrogen production from carbon dioxide reforming of methane over highly active and stable MgO promoted Co-Ni/α-Al_2O_3 catalyst. *Int. J. Hydrog. Energy*, 2014, **39**, P. 3762–3770.

[31] Xu J., Zhou W., Li Z., Wang J., Ma J. Biogas reforming for hydrogen production over nickel and cobalt bimetallic catalysts. *Int. J. Hydrog. Energy*, 2009, **34**, P. 6646–6654.

[32] Foo S.Y., Cheng C.K., Nguyen T-H., Adesina A.A. Oxidative CO_2 reforming of methane on alumina-supported Co–Ni catalyst. *Ind. Eng. Chem. Res.*, 2010, **49**, P. 10450–10458.

[33] Fan M-S., Abdullah A.Z., Bhatia S. Utilization of greenhouse gases through carbon dioxide reforming of methane over Ni–Co/MgO-ZrO_2: preparation, characterization and activity studies. *Appl. Catal. B: Environ.*, 2010, **100**, P. 365–377.

[34] Halliche D., Bouarab R., Cherifi O., Bettahar M.M. Carbon dioxide reforming of methane on modified Ni/α-Al_2O_3 catalysts. *Catal. Today*, 1996, **29**, P. 373–377.

[35] San-Jose-Alonso D., Illan-Gomez M.J., Roman-Martınez M.C. Low metal content Co and Ni alumina supported catalysts for the CO_2 reforming of methane. *Int. J. Hydrog. Energy*, 2013, **38**, P. 2230–2239.
[36] Wu Z., Yang B., Miao S., Liu W., Xie J., Lee S.,. Pellin M.J, Xiao D., Su D., Ma D. Lattice strained Ni–Co alloy as a high-performance catalyst for catalytic dry reforming of methane. *ACS Catal.*, 2019, **9**, P. 2693–2700.
[37] San-Joze-Alonso D., Juan-Juan J., Illan-Gomez M.J., Roman-Martinez M.C. Ni, Co and bimetallic Ni–Co catalysts for the dry reforming of methane. *Appl. Catal. A: Gen.*, 2009, **371**, P. 54–59.
[38] Kumari R., Sengupta S. Catalytic CO_2 reforming of CH_4 over $MgAl_2O_4$ supported Ni–Co catalysts for the syngas production. *Int. J. Hydrog. Energy*, 2020, **45**, P. 22775–22787.
[39] Li H., Shin K., Henkelman G. Effects of ensembles, ligand, and strain on adsorbate binding to alloy surfaces. *J. Chem. Phys.*, 2018, **149**, 174705.
[40] Khairudin N.F., Mohammadi M., Mohamed A.R. An investigation on the relationship between physicochemical characteristics of alumina-supported cobalt catalysts and its performance in dry reforming of methane. *Environ. Sci. Pollut. Control Ser.*, 2021, **28** (23), P. 29157–29176.
[41] Dekkar S., Tezkratt S., Sellam D., Ikkour K., Parkhomenko K., Martinez-Martin A., Roger A.C. Dry reforming of methane over Ni–Al_2O_3 and Ni–SiO_2 catalysts: role of preparation methods. *Catal. Lett.*, 2020, **150**, P. 2180–2199.
[42] *TOPAS V4.2: General Profile and Structure Analysis Software for Powder Diffraction Data – User's Manual*; Bruker AXS: Karlsruhe, Germany, 2008; Available online: (http://algol.fis.uc.pt/jap/TOPAS %204-2 %20Users %20Manual.pdf (accessed on 8 May 2020))
[43] Database: Inorganic Crystal Structure Database, ICSD. In Release 2008. Fashinformationszentrum Karsruhe D #8211 1754 Eggenstein #8211 Leopoldshafen, Germany, 2008.
[44] Moudler J., Stickle W., Sobol P., Bomben K., *Handbook of X-ray Photoelectron Spectroscopy*, Perkin-Elmer Corp.: Eden. Prairie, MN, 1992.
[45] Scofield J.H., *J. Electron Spectrosc. Relat. Phenom.*, 1976, **8**, P. 129–137.
[46] Kwok R. Free, fully featured, software for the analysis of XPS spectra. November 25, 2023, http://xpspeak.software.informer.com/4.1/ .
[47] Ji Y., Zhao Z., Duan A., Jiang G., Liu J. Comparative study on the formation and reduction of bulk and Al_2O_3-supported cobalt oxides by H_2-TPR technique. *Phys. Chem. C*, 2009, **113**, P. 7186–7199.
[48] Andonova S., de Avila C.N., Arishtirova K., Bueno J.M.C., Damyanova S. Structure and redox properties of Co promoted Ni/Al_2O_3 catalysts for oxidative steam reforming of ethanol. *Appl. Catal. B: Environ.*, 2011, **105**, P. 346–360.
[49] Wang R., Li Y., Shi R., Yang M. Effect of metal-support interaction on the catalytic performance of Ni/Al_2O_3 for selective hydrogenation of isoprene. *J. Mol. Catal. A: Chem.*, 2011, **344**, P. 122–127.
[50] Zhang H.J., Chen Z.Q., Wang S.J. Spin conversion of positronium in NiO/Al_2O_3 catalysts observed by coincidence Doppler broadening technique. *Phys. Rev. B*, 2010, **82**, 035439.
[51] Gao Y., Qiao F., Hou W., Ma L., Li N., Shen C., Jin T., Xie K. Radiation effects on lithium metal batteries. *The Innovation*, 2024, **3**, 100468.
[52] Du J., Liu G., Li F., Zhu Y., Sun Iron–Salen L. Complex and Co^{2+} Ion-Derived Cobalt–Iron Hydroxide/Carbon Nanohybrid as an Efficient Oxygen Evolution. *Electrocatalyst. Adv. Sci.*, 2019, **6**, 1900117.
[53] Li C., Li S., Zhao J., Sun M., Wang W., Lu M., Qu A., Hao C., Chen C., Xu C., Kuang H., Xu L. Ultrasmall Magneto-chiral Cobalt Hydroxide Nanoparticles Enable Dynamic Detection of Reactive Oxygen Species in Vivo. *JACS*, 2022, **144**, P. 1580–1588.
[54] Cano A.M., Marquardt A.E., DuMont J.W., George S.M. Effect of HF Pressure on Thermal Al_2O_3 Atomic Layer Etch Rates and Al_2O_3 Fluorination. *J. Phys. Chem. C*, 2019, **123**, P. 10346–10355.
[55] Huang L., Xiong K., Wang X., He X., Yu L., Fu C., Zhu X., Feng W. The Mechanism of Oxide Growth on Pure Aluminum in Ultra-High-Temperature Steam. *Metals*, 2022, **12**, 1049
[56] Misture S.T., McDevitt K.M., Glass K.C., Edwards D.D., Howe J.Y., Rector K.D.,H. He, Vogel S.C., Sulfur-resistant and regenerable Ni/Co spinel-based catalysts for methane dry reforming. *Catal. Sci. Technol.*, 2015, **5**, P. 4565–4574.
[57] Li B., Luo Y., Li B., Yuan X., Wang X. Catalytic performance of iron-promoted nicel-based ordered mesoporous alumina FeNiAl catalysts in dry reforming of methane. *Fuel Process. Technol.*, 2019, **193**, P. 348–360.
[58] Alipour Z., Rezaei M., Meshkani F. Effects of support modifiers on the catalytic performance of Ni/Al_2O_3 catalyst in CO_2 reforming of methane. *Fuel*, 2014, **129**, P. 197–203.

Submitted 5 September 2024; revised 28 November 2024; accepted 5 December 2024

Information about the authors:

Alexey A. Shutilov – Boreskov Institute of Catalysis SB RAS, Lavrentieva 5, Novosibirsk 630090, Russia; ORCID 0009-0008-1682-1125; alshut@catalysis.ru

Mikhail N. Simonov – Boreskov Institute of Catalysis SB RAS, Lavrentieva 5, Novosibirsk 630090, Russia; Novosibirsk State University, Pirogova 2, Novosibirsk 630090, Russia; ORCID 0000-0002-5161-5684; smike@catalysis.ru

Valeria E. Fedorova – Boreskov Institute of Catalysis SB RAS, Lavrentieva 5, Novosibirsk 630090, Russia; ORCID 0000-0002-0551-1892; valeria@catalysis.ru

Alexander S. Marchuk – Novosibirsk State University, Pirogova 2, Novosibirsk 630090, Russia; ORCID 0000-0003-4063-5142; alexander.s.marchuk@gmail.com

Igor P. Prosvirin – Boreskov Institute of Catalysis SB RAS, Lavrentieva 5, Novosibirsk 630090, Russia; ORCID 0000-0002-0351-5128; prosvirin@catalysis.ru

Galina A. Zenkovets – Boreskov Institute of Catalysis SB RAS, Lavrentieva 5, Novosibirsk 630090, Russia; ORCID 0000-0002-3896-8071; zenk@catalysis.ru

Conflict of interest: the authors declare no conflict of interest.